Acta Cryst. (1998). D**54**, 313–323

1.85 Å Resolution Structure of the Zinc^{II} β-Lactamase from *Bacillus cereus*

ANDREA CARFI,[a] EMILE DUÉE,[a] MORENO GALLENI,[b] JEAN-MARIE FRÈRE[b] AND OTTO DIDEBERG[a]*

[a]*LCM, Institut de Biologie Structurale Jean-Pierre Ebel (CEA-CNRS), Grenoble, France, and* [b]*Centre d'Ingénierie des Protéines, Université de Liège, Liège, Belgium. E-mail: otto@ibs.fr*

(*Received 23 April 1997; accepted 28 July 1997*)

Abstract

Class B β-lactamases are wide-spectrum enzymes which require bivalent metal ions for activity. The structure of the class B zinc-ion-dependent β-lactamase from *Bacillus cereus* (BCII) has been refined at 1.85 Å resolution using data collected on cryocooled crystals (100 K). The enzyme from *B. cereus* has a molecular mass of 24 946 Da and is folded into a β-sandwich structure with helices on the external faces. The active site is located in a groove running between the two β-sheets [Carfi *et al.* (1995). *EMBO J.* **14**, 4914–4921]. The 100 K high-resolution BCII structure shows one fully and one partially occupied zinc site. The zinc ion in the fully occupied site (the catalytic zinc) is coordinated by three histidines and one water molecule. The second zinc ion is at 3.7 Å from the first one and is coordinated by one histidine, one cysteine, one aspartate and one unknown molecule (which is most likely to be a carbonate ion). In the *B. cereus* zinc β-lactamase the affinity for the second metal ion is low at the pH of crystallization [K_d = 25 m*M*, 293 K; Baldwin *et al.* (1978). *Biochem. J.* **175**, 441–447] and the dissociation constant of the second zinc ion thus apparently decreased at the cryogenic temperature. In addition, the structure of the apo enzyme was determined at 2.5 Å resolution. The removal of the zinc ion by chelating agents causes small changes in the active-site environment.

1. Introduction

The targets of β-lactam-based antibiotics are the membrane-bound transpeptidases (PBP's, Spratt, 1975), which are involved in the synthesis of the cell-wall peptidoglycan. Inactivation of the transpeptidases leads to cell lysis or production of deformed cells. Bacteria have developed various strategies to escape the action of antibiotics. The primary resistance mechanism is the production of β-lactamases, membrane-bound, periplasmic or extracellular enzymes which cleave the β-lactam ring. Nevertheless, because of their low cost of production and their minimal side effects (Neu, 1992) the antibiotics of the β-lactam family are still the most widely used to fight pathogenic bacterial infections. On the basis of their amino-acid sequences β-lactamases have been divided into four classes, A to D (Ambler, 1980). In the enzymes of classes A, C and D a serine residue is responsible for the attack on the carbonyl C atom of the β-lactam ring. In class B a water molecule, polarized by the zinc ion, probably acts as a nucleophile. The serine β-lactamases have been studied for a long time and several high-resolution structures of class A and C enzymes have been reported: the class A β-lactamases from *Staphylococcus aureus* (Herzberg, 1991), *Bacillus licheniformis* (Knox & Moews, 1991), and TEM-1 (Strynadka *et al.*, 1992; Jelsch *et al.*, 1993; Fonzé *et al.*, 1995); the class C β-lactamase from *Citrobacter freundii* (Oefner *et al.*, 1990) and *Enterobacter cloacae* P99 (Lobkovsky *et al.*, 1993). All these enzymes are characterized by a two-domain structure with the active-site serine lying at the bottom of a crevice located at their interface. The serine β-lactamase and the PBP's are evolutionary related (Kelly *et al.*, 1986; Samraoui *et al.*, 1986) and share three conserved active-site signatures S*XX*K, S(Y)*X*N and KT(S)G. However, despite the large number of mutagenesis studies, their catalytic mechanism remains controversial.

The third-generation cephalosporins and carbapenems (*e.g.* imipenem), generally escape the action of the most common serine β-lactamases except for some mutants of the TEM family (Knox, 1995) and the recently discovered class A carbapenemases, and several efficient inhibitors of these enzymes are in clinical use. In the last few years there has been an increasing interest for class B β-lactamases, since some pathogenic bacteria were found to produce this type of enzyme. Class B enzymes have no sequence or structural similarity with the active-site serine enzymes and require a bivalent metal ion for activity: for the *Bacillus cereus* II enzyme the Co^{2+}-, Ni^{2+}-, Cd^{2+}- and Mn^{2+}-substituted proteins are active while Hg^{2+} and Cu^{2+} inactivate the enzyme (Davies & Abraham, 1974). The fact that most zinc β-lactamases hydrolyze almost all the antibiotics of the penicillin family and that no clinically useful inhibitors are presently available makes these enzymes important targets for drug design. The elucidation of the three-dimensional structure of the Zn^{2+} β-lactamase from *B. cereus* (BCII) at 2.5 Å resolution and 300 K (Carfi *et al.*, 1995) has shown that

these enzymes represent a new protein structural family. Later two structures of the zinc-β-lactamase of *Bacteroides fragilis* have been reported (Concha *et al.*, 1996; Carfi *et al.*, 1998). A comparison between BCII and *B. fragilis* β-lactamase active sites has supplied the structural basis for understanding their different metal requirements. Here we present the low-temperature (100 K) 1.85 Å refined structure of BCII together with the structure of the metal-depleted enzyme.

2. Materials and methods

2.1. *Crystallization and cryocooling*

Monoclinic *C*2 crystals were grown at 281 K by the hanging-drop vapour-diffusion method. Drops were prepared by mixing equal volumes of a 9 mg ml^{-1} protein solution in 10 m*M* cacodylate pH 6.5, 100 μ*M* dithiothreitol (DTT), 100 μ*M* $ZnAc_2$, and reservoir buffer. The reservoir solution contained 25 m*M* citrate pH 5.6, 20% polyethylene glycol 8000 (PEG 8 K), 100 μ*M* $ZnAc_2$, 100 μ*M* DTT. The apoenzyme crystals were obtained by washing the holoprotein crystals for 3 d against a reservoir buffer containing 1 m*M* EDTA and no Zn^{2+}. Measured at 300 K, they are in space group *C*2 with one molecule per asymmetric unit and cell parameters a = 53.8, b = 63.2, c = 70.1 Å, β = 93.5°.

For synchrotron data collection at cryogenic temperature, the holo BCII crystals were soaked for 5 min in a solution of the same composition as that of the reservoir except for the presence of 20%(*v*/*v*) glycerol as cryoprotectant (Rodgers, 1994). Next, crystals were mounted on a nylon loop and flash frozen by immersion in liquid nitrogen. The frozen crystals have unit-cell dimensions a = 53.00, b = 61.35, c = 69.45 Å, β = 92.93°, space group *C*2 with one molecule per asymmetric unit.

By comparison with the holo BCII crystals at 300 K (Carfi *et al.*, 1995), a variation of the unit-cell volume of about 3% is observed, corresponding to a contraction for the holo BCII crystals at 100 K and to an expansion for the apo BCII crystals at 300 K.

2.2. *Data collection and refinement*

The 2.5 Å resolution model (Carfi *et al.*, 1995) was initially refined to 2.2 Å with data collected in house on a Mar Research imaging plate on a cryocooled crystal (100 K) (data set 1, Table 1). Later, a 1.85 Å data set collected on a CCD detector at the D2AM line (ESRF, Grenoble), became available (data set 2, Table 1). The data were indexed and integrated with *XDS* (Kabsch, 1988). As a result of oversaturation, the synchrotron data were only 50% complete between infinity and 2.8 Å. For this reason data sets 1 and 2 were merged using the program *SCALA* (*CCP*4 suite, Collaborative Computational Project, Number 4, 1994). Because the R_{merge} increased with the resolution when all the data were merged, only the data between infinity and 2.8 Å from data set 1 were used to supplement data set 2, resulting in the final data set (data set 3, Table 1) with a good completeness over the whole resolution range. Data statistics are summarized in Table 1. The *CCP*4 suite was used for further processing of the data.

Table 1. *Data collection of the native enzyme*

Resolution (Å)	Data set 1 R_{sym}/% poss.†	Data set 2 R_{sym}/% poss.	Data set 3‡ R_{sym}/% poss.
6.87	0.037/94.5	0.056/32.3	0.039/94.1
4.90	0.043/99.7	0.066/56.1	0.053/98.7
4.01	0.048/97.8	0.073/44.3	0.043/98.5
3.48	0.053/99.8	0.071/52.0	0.056/100.0
3.11	0.059/99.3	0.056/41.4	0.048/99.6
2.84	0.070/100.0	0.060/69.9	0.089/100.0
2.63	0.079/100.0	0.065/97.4	0.065/97.4
2.46	0.100/99.4	0.064/99.3	0.064/99.3
2.32	0.108/99.2	0.064/99.4	0.064/99.4
2.20	0.115/97.1	0.060/96.3	0.060/96.3
2.10	0.117/88.9	0.065/95.8	0.065/95.8
2.01	–	0.075/91.4	0.075/91.4
1.93	–	0.088/84.8	0.088/84.8
1.85	–	0.104/77.7	0.104/77.7
Overall	0.06/98.5	0.07/80.9	0.07/94.6

† % poss. = completeness. ‡ Data set 3 is the data set 2 supplemented with low-resolution data (∞–2.8 Å) measured in data set 1 (see §2).

After an initial rigid-body refinement the model was refined using the slow-cool procedure of *X-PLOR* (Brünger, 1992*a*) (starting temperature 3000 K) followed by several cycles of positional refinement and individual *B*-factor refinement. 5% of the reflections were used for the R_{free} calculation (Brünger, 1992*b*). Surprisingly the ($2|F_o| - |F_c|, \alpha_c$) electron-density map showed a strong density (above 5σ) approximately 3.5 Å from the first zinc ion, indicating the presence of a second zinc ion. Corroborating evidence included the composition of the crystallization solution, metal–ligand distances and biochemical data (Davies & Abraham, 1974; Baldwin *et al.*, 1978) as well as comparison with the enzyme from *B. fragilis* which tightly binds two zinc ions in equivalent sites (Concha *et al.*, 1996; Carfi *et al.*, 1998). For BCII the dissociation constant for the second metal ion at the pH of crystallization and at 293 K was reported to be 25 m*M* (Baldwin *et al.*, 1978) and it is likely that the low temperature stabilized the binding of Zn^{2+} at this site.

Charged residues and zinc ions were refined as neutral and no restraints of any kind were applied between the metal ions and their ligands. Once the *R* factor had been reduced from the initial value of 38.5 to 26.5%, water molecules were added. The *ARP* program (Lamzin & Wilson, 1993) was used to localize water molecules which were included only if present at above 3σ in the ($|F_o| - |F_c|$) difference electron-density map and in satisfactory positions to make hydrogen bonds with neighboring atoms. For model building the

program *O* was used (Jones *et al.*, 1991). The occupancy of the second metal ion was evaluated at 0.6 to keep its *B* factor close to that of its ligands. At the end of the refinement a planar triangular shaped density [at 1.5σ in the $(2|F_o| - |F_c|, \alpha_c)$ map] was persisting in the active site on the solvent side of the second zinc ion. This unknown molecule was interpreted as a carbonate ion, based on the shape of the electron density together with the hydrogen-bond interactions with neighbouring atoms. For the structure of the apoenzyme two data sets were collected at room temperature on a FAST area detector (2.5 and 2.8 Å resolution, respectively). The 2.5 Å data set was used for refinement, starting with the holo BCII structure refined at 2.2 Å resolution (see above) as the model. In the σ-weighted $2|F_o| - |F_c|$ maps a break was observed in the main chain of helix α_2. Assuming that the problem was caused by the incompleteness of the data at low resolution, the low-resolution (infinity to 5 Å) reflections which were missing in the 2.5 Å data set were added with the amplitudes measured in the 2.8 Å data set after scaling with *SCALEIT* (Collaborative Computational Project, Number 4, 1994) (the two data sets could not be thoroughly merged because of a slight lack of isomorphism which affected data at higher resolution). This completed data set was used only for computing the maps, which no longer presented gaps.

2.3. *Quality of the models*

In both structures, apo and 2Zn form, there was no interpretable density for residues 32–39 (between β_3 and β_4) and no density was observed for the six N-terminal residues. The average *B* factors for the 25 N-terminal residues are higher than for the rest of the structure (30 against 20 Å^2 in the 1.85 Å structure) indicating that this region is flexible. The density for residues 11–13 (between β_1 and β_2) is stronger in the case of the apoenzyme.

2.4. *Assessment of structure quality*

The models were examined using the *PROCHECK* program (Laskowski *et al.*, 1993). They show good geometry, all parameters being consistent with those observed in other high-resolution structures. All main-chain dihedral angles fall within allowed regions of the Ramachandran plot (Fig. 1) (Ramachandran *et al.*, 1963) except for Asp56, which was modelled with unfavourable dihedral angles ($\varphi = 76°$, $\psi = 145°$). This residue is at the end of a β-strand and close to the active-site, and makes a salt bridge with Arg91. The importance and the interactions of these residues in BCII will be discussed below. The final 2Zn enzyme model contains 213 amino acids (out of 227), two Zn atoms, one carbonate ion and 214 water molecules which were refined with a *B* factor <50 Å^2. The final *R* factor is 0.214 for 17 705 reflections in the resolution range 8–1.85 Å and the R_{free} factor is 0.262. The r.m.s. deviation from ideality for bond lengths is 0.014 Å and for bond angles it is 1.52°.

Table 2. *Refinement statistics of the holo and apoenzyme*

	Holo 1.85 Å (100 K)	Apo 2.50 Å (300 K)
Resolution range (Å)	8–1.85	10–2.5
No. of reflections†	17705	7535
R_{cryst} (%)	0.214	0.206
R_{free} (%)	0.262	0.264
R.m.s.d. (Å)	0.014	0.018
R.m.s.d. (°)	1.52	1.82
No. of residues	213	213
No. water molecules	214	28
Ions	2 Zn^{2+}, 1 CO_3^{2-}	—

† With $F > 2\sigma(F)$.

The final apoenzyme model includes 213 amino acids, 28 water molecules and the *R* factor is 0.206 for 7535 reflections in the resolution range 10–2.5 Å and R_{free} is 0.264. The refinement statistics are summarized in Table 2.

3. Results and discussion

3.1. *Chain fold and secondary structure*

The secondary-structure assignments (Fig. 2) made using the *Hera* program (Hutchinson & Thornton, 1990) confirm and extend the description given at lower resolution (Carfi *et al.*, 1995). BCII is a β-sandwich structure with helices on the external faces. Two domains can be defined. The N-terminal domain is

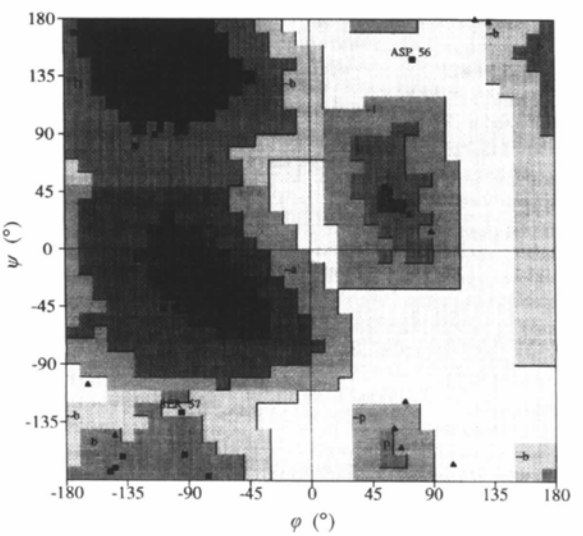

Fig. 1. Ramachandran plot calculated using *PROCHECK* (Laskowski *et al.*, 1993). Glycine residues are shown as triangles and the other residues as squares. The Asp56 residue with conformational angles outside allowed regions is labeled.

constituted of seven β-strands and three helices: $\beta_1\beta_2\beta_3\beta_4\beta_5$ are antiparallel and $\beta_5\beta_6\beta_7$ are parallel. In the C-terminal domain there are five β-strands and two helices: $\beta_8\beta_9\beta_{10}\beta_{11}$ are antiparallel and $\beta_{11}\beta_{12}$ are parallel. The active site is located on the top of the sandwich in a long channel between the two β-sheets. The two domains are connected by eight residues (121–128) devoid of secondary structure. The only other known zinc β-lactamase structure, from the pathogenic *Bacteroides fragilis* (Concha *et al.*, 1996; Carfi *et al.*, 1998) has a very similar structure. Fig. 3 shows that in BCII there are two short insertions at the N-terminus and the C-terminal helix is shorter than in the *B. fragilis* β-lactamase. The insertions are located in the loops between β-strands β_1–β_2 and β_3–β_4. These loops are disordered in BCII (see above) and stabilized by packing contacts in both *B. fragilis* β-lactamase structures. From a superposition of *B. cereus* and *B. fragilis* β-lactamase structures (Fig. 4) it can be noted that the largest differences are in the conformation of protein regions connecting secondary-structure elements and in the ten-residue sequence following α_3 which has no secondary structure in BCII but is a β-strand (β_8) in *B. fragilis*. If these residues are excluded the r.m.s.d. for 120 Cα is 0.85 Å. The protein secondary-structure elements superpose very well with the exception of β-strands β_9 and β_{10} in BCII with the corresponding β_{10} and β_{11} in *B. fragilis*. These β-strands interact by main-chain hydrogen bonds and, near their C-terminus, through a conserved buried water molecule. It is likely that in the *B. fragilis* enzyme the K135P mutation, a residue close to this buried water molecule, is responsible for this movement together with differences in the packing interactions. In fact in the *B. fragilis* β-lactamase crystals the protein dimerize through the interaction of β_8 and β_9 (Carfi *et al.*, 1998) and these interactions could have an effect on the positioning of β_{10}.

3.2. *Metal coordination*

The ligand sphere of the fully occupied site (Zn1) has the characteristics of the catalytically active zinc ions

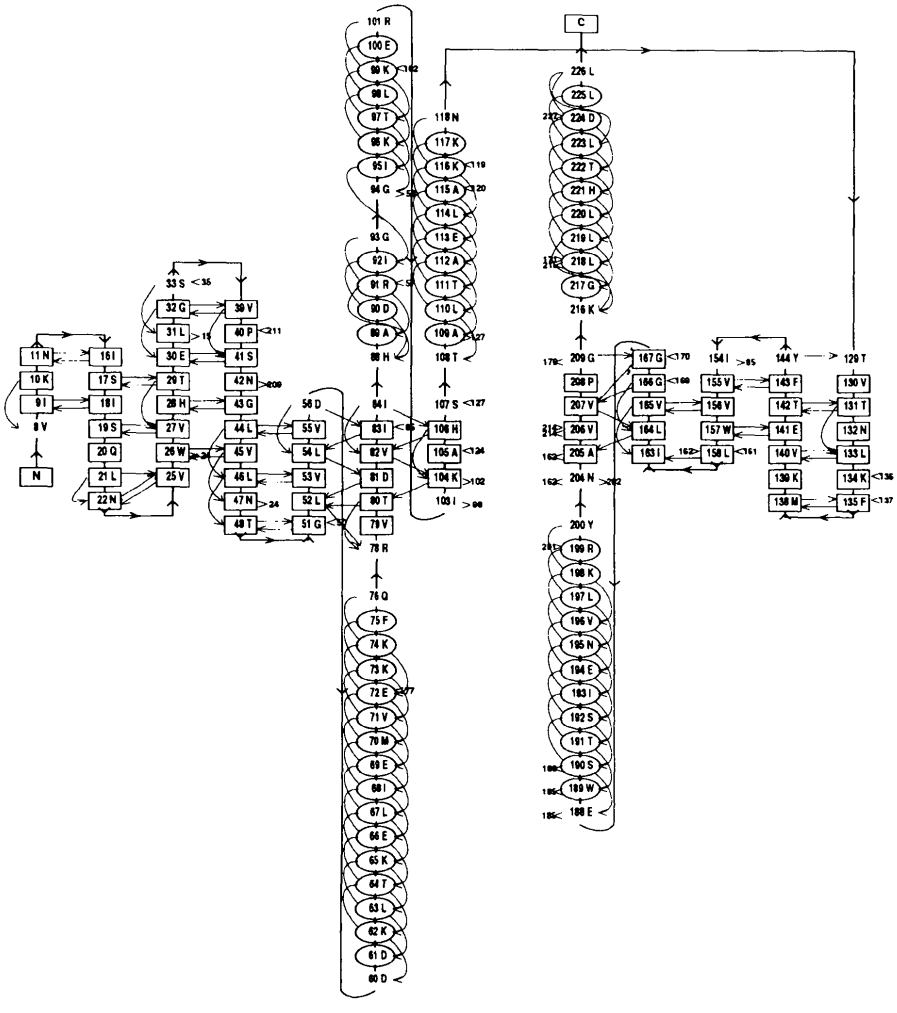

Fig. 2. Secondary structure and hydrogen bonding within the *B. cereus* β-lactamase structure. The diagram was prepared using the program *HERA* (Hutchinson & Thornton, 1990). The flexible loop (32–39) has been modelled on the basis of the *B. fragilis* β-lactamase structure.

(Vallee & Auld, 1993) with two histidines (His86 and His88) separated by one amino acid and a third histidine (His149) separated by a long spacer of 60 amino acids. A water molecule (Wat1), 2.25 Å from the Zn^{2+}, completes the coordination of the zinc ion. The second metal ion (Zn2) is 3.74 Å from the first one and is coordinated by Asp90 OD2, Cys16 SG, and His210 ND1 (Fig. 5). The protein zinc ligands are found

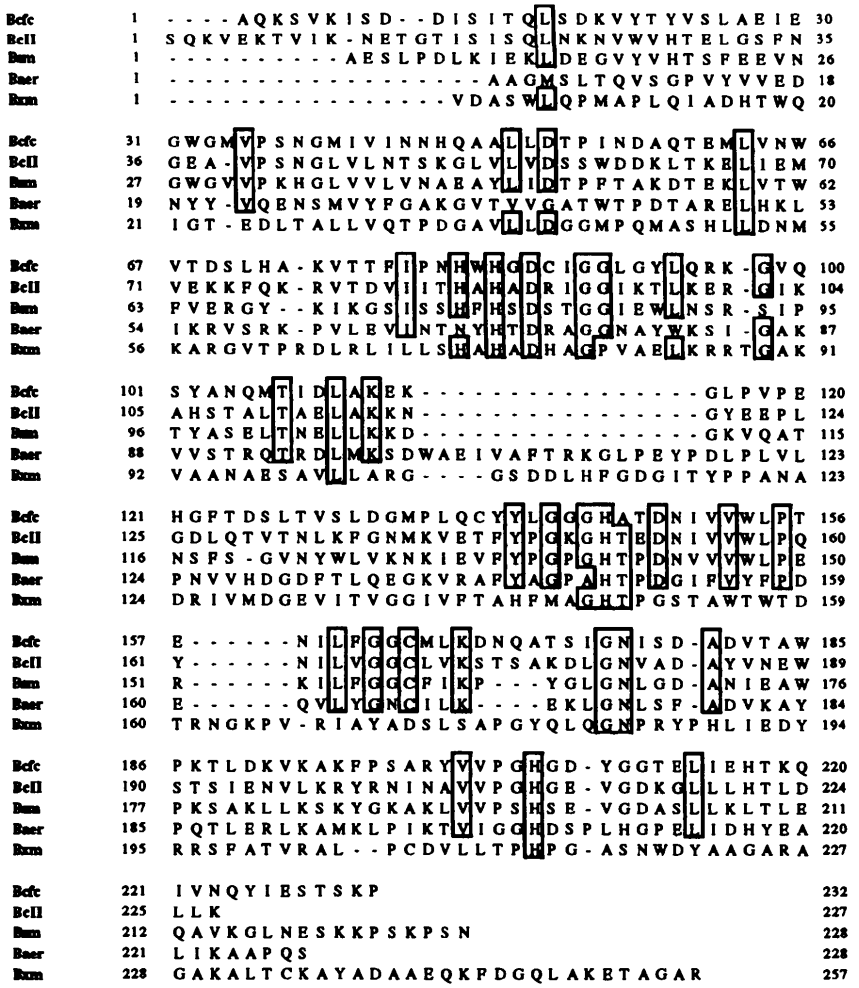

Fig. 3. Sequence alignment for some class B enzymes. For the *B. cereus* and *B. fragilis* metallo-β-lactamases the alignment is based on the superposed crystallographic structures. For the other sequences the alignment was made as described in Carfi *et al.* (1995). Sequences are: Bcfc, *B. fragilis* (Rasmussen *et al.*, 1990; Thompson & Malamy, 1990); BCII, *B. cereus* (569/H/9) (Ambler *et al.*, 1985; Hussain *et al.*, 1985; Kato *et al.*, 1985); Bsm, *S. marcescens* (Osano *et al.*, 1994); Baer, *A. hydrophila* (Massida *et al.*, 1991); Bxm, *Stenotrophomonas* (previously *Xanthomonas*) *maltophilia* (Walsh *et al.*, 1994).

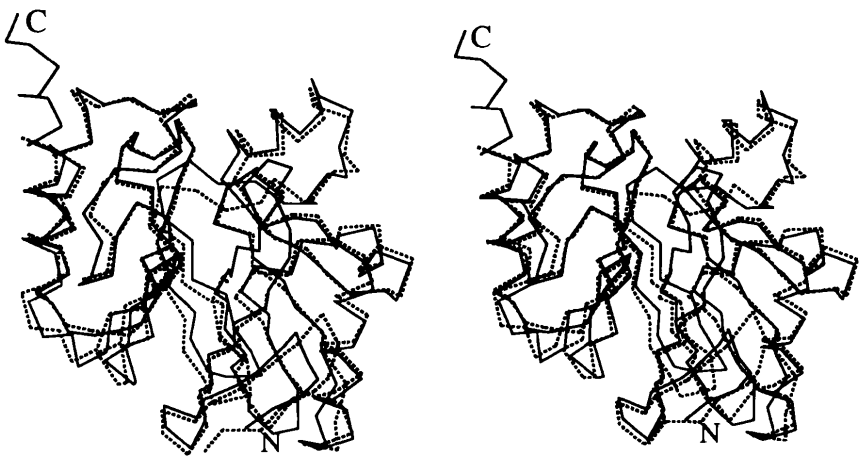

Fig. 4. Stereoview of the Cα superposition of the *B. cereus* (dotted lines) and *B. fragilis* (solid lines) Zn^{II} β-lactamases. Figs. 4, 8, and 9 were obtained using *MOLSCRIPT* (Kraulis, 1991).

in the following order along the sequence: His86, His88 and Asp90 at the N-terminal of the helix α_2, His149 between β_9 and β_{10}, Cys168 and His210 at the C-terminus of β_{11} and β_{12}, respectively (Fig. 2). On the solvent side of the second zinc an initially uninterpreted electron density was assigned to a carbonate ion (Fig. 5). The carbonate ion binds Zn2 as a bidentate ligand ($OT1_{car}\cdots Zn2$ = 2.8 Å; $OT2_{car}\cdots Zn2$ = 2.9 Å). Moreover, those two carbonate O atoms make two hydrogen bonds: one O atom with the Zn1-bound water molecule (Wat1) and the second one with a surface water molecule. The third O atom is hydrogen bonded to Asn180 N. The second zinc and the carbonate ions have been refined with the same occupancy (0.6) and show similar *B* factors ($\simeq$ 22 Å^2).

In the present structure the two zinc ions are tetra and pentacoordinated, respectively, and no water molecules or protein residues are shared by the two metals (Table 3). The metal coordination geometry can be described as tetrahedral for Zn1 and as square bipyramidal for Zn2, with however an apex missing in the direction of the other zinc. It is interesting to observe that all protein zinc ligands are strictly conserved in the class B enzymes (Fig. 3) with the exception of two mutations His88→Asn in the *Aeromonas* enzyme and Cys168→Asp in the *Stenotrophomonas maltophilia* enzyme (previously *Xanthomonas*). In the room-temperature structure (Carfi *et al.*, 1995) a weak density, in a position equivalent to that occupied by the second zinc ion in the 100 K model, was assigned to a water molecule (WatA) (Table 3 for metal–water ligand distances). The presence of the second metal ion was not expected in the present crystallization conditions (*i.e.* pH = 5.7 and 100 μ*M* $ZnAc_2$; K_{dZn2} = 25 m*M* at 293 K; Baldwin *et al.*, 1978) and in the 1.85 Å structure the binding of Zn^{2+} to this site was probably favoured by the low temperature. Indeed, the dissociation of the sulfydryl group is exothermic and one would thus expect the pK_a of this group to decrease at low temperature. The relatively high *B* factor and the partial occupancy for the second zinc ion indicate that this metal ion is not tightly bound.

Table 3. *Metal–ligand distances (Å) at 100 K and room temperature (300 K)*

Protein	Zn^{II}/WatA	1.85 Å (100 K)	2.50 Å (300 K)
His86 NE2	Zn1	2.32	2.36
His88 ND1	Zn1	2.21	2.34
His149 NE2	Zn1	2.27	2.40
Wat1	Zn1	2.25	2.31
Asp90 OD1	Zn2/WatA†	2.32	2.46
Cys168 SG	Zn2/WatA†	2.31	2.69
His210 NE2	Zn2/WatA†	2.41	2.78
CO_3^{2-}(1)	Zn2/WatA†	2.95	–
CO_3^{2-}(2)	Zn2/WatA†	2.85	–
Arg91 NH2	Zn2/WatA†	4.19	4.45
Zn1	Zn2/WatA†	3.74	3.43

† Zn2 is present in the structure at 100 K. Near its position the water molecule WatA is observed in the structure at 300 K.

In the mercury-substituted enzyme (Carfi *et al.*, 1995), in spite of the fact that a cysteine ligand is present in the active site, only one mercury ion was found, replacing the zinc ion at the high-affinity site. A possible explanation for these observations is the partial protonation, at the pH of crystallization, of the cysteine and histidine ligands and the active-site electrostatic environment (see below). In the case of the mercury-substituted enzyme the large radius of the mercury ion together with a partial oxidation of Cys168 (see below) could result in the binding of only one metal ion.

3.3. *The catalytic site in the holoenzyme*

The catalytic site of BCII is located at the bottom of a 10 Å wide groove running between the two β-sheets. Two loops 32–39 and 174–185 flank the active-site channel. The flexible 32–39 loop is disordered in the BCII structure but has been modelled on the basis of the *B. fragilis* β-lactamase structure (Carfi *et al.*, 1998). The other side of the zinc-binding site is polar with two aspartates (D177 and D183) and one asparagine (N180) pointing into the channel. Another charged residue Lys171 is lying at the bottom of the active site with its side chain oriented to the second metal ion. There is a

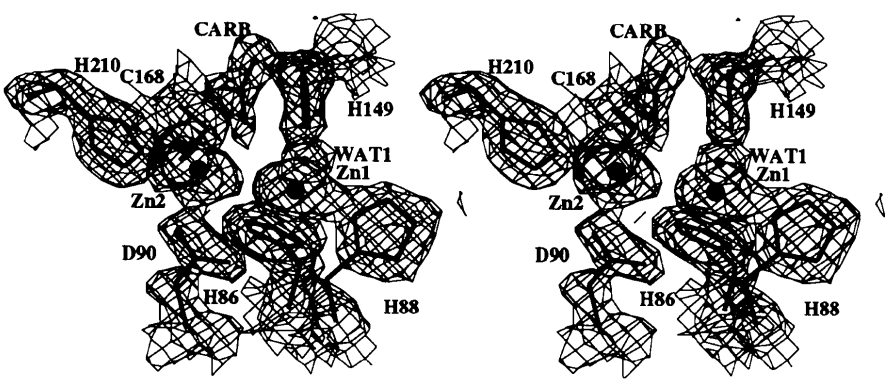

Fig. 5. Stereoview of the zinc ions and their ligands. The electron-density map is contoured at 1.3σ level. The figure was obtained using the program *O*.

complex hydrogen-bonding network in the active site involving interactions between water molecules, the zinc ions, the carbonate ion and the polar residues.

Each zinc-ligand side chain, except Cys168, makes interactions with a protein atom or with structural water molecules: His86 ND1···Wat7, His88 NE2 ···Asp183 OD2, His149 NE2···Wat10, Asp90 OD2··· Arg91 NH2, His210 ND1···Pro40 O. Wat7 is in turn hydrogen bonded to Thr85 OG1 and Wat10 hydrogen bonds Asn180 O and Leu178 O (see below). Many polar and charged residues are located in the interior of the protein close to the active site: His28, Glu30, Ser41, Asn42, Asp56, Thr85, Arg91, Thr108, Thr111, Thr150, Asp152 and Asn153. These residues make hydrogen bonds with protein atoms or buried water molecules. The resulting pattern of hydrogen bonds is important for the positioning of residues located in the part of the protein devoid of secondary structure (*e.g.* His149, His210, Cys168 and Asn180) (Fig. 2). Eight buried water molecules stabilize the protein structure (Table 4) and indirectly contribute to the active-site architecture. The side chain of Asn153 interacts with three residues, His149 N, Thr150 N and Gly146 O, and its main-chain N-atom hydrogen bonds Thr150 OG1. The carboxylate of Asp152 makes three hydrogen bonds with Thr150 OG1, Thr111 OG1 and Ala87 N (next to His86, His88 and Asp90 in α_2), respectively. Four other charged residues are buried in the structure and are involved in salt bridges: His28, Glu30, Asp56 and Arg91. Glu30 (β_3) makes a salt bridge with His28 (β_3) and hydrogen bonds Wat2. The other two residues, Asp56 and Arg91 are strategically positioned near the active site. The guanidinium group of Arg91 is maintained between Asp90 and Asp56 (Arg9 ND1 ···Asp90 OD2 and Arg91 ND2···Asp56 OD2 = 2.9 Å) and hydrogen bonds Wat4, Asn42 O and Gly209 O. The carboxylate of Asp56 in turn makes four additional hydrogen bonds: two hydrogen bonds with Thr85 OG1, one with Thr85 N (α_2) and a fourth with Wat4. Wat6 and Wat10 hold the 174–185 loop (containing Asn180). Two residues, Asp152 and Asn153, orient the short 147–152 loop (between β_9 and β_{10}) containing the zinc ligand His149. Wat7 and Wat8 stabilize the zinc ligands Cys168 and His86. It is important to observe that the guanidinium group of Arg91 is only 4.2 Å away from the second zinc ion. The close proximity of this positive charge to the second zinc site may explain the low affinity for the second metal ion in BCII. When conserved, this residue is expected to have the same effect on the metal binding at the second zinc site (*e.g.* in *A. hydrophila* metallo-β-lactamase). Fig. 6 shows views of the active sites of the BCII and *B. fragilis* zinc β-lactamases in the same orientation. Two mutations are especially important: the large and positively charged Arg91 (in BCII) is replaced by the small Cys87 and Thr85 by Asn81. In the *B. fragilis* β-lactamase the effects of these mutations are compensated by the presence of a sodium ion and by a somewhat different disposition of the buried water molecules (Table 4): the guanidinium group of Arg91 in BCII occupies a position equivalent to that of the Na^+ ion in the *B. fragilis* β-lactamase; the buried water molecule Wat7 in BCII is replaced by the side chain of Asn81 OD1; Asp86 OD2 (Asp90 in *B. cereus* numeration) is hydrogen bonded to a sodium-bound water molecule (Wat1) which replaces Arg91 NH2 of BCII. It is important to observe that the Na^+ ion, even if it occupies a position structurally equivalent to that of the charged guanidinium group of Arg91, is 6.0 Å away from Zn2 and has therefore a smaller repulsive effect.

Table 4. *Description of the internal water molecules in B. cereus β-lactamase II*

Cavity in BCII	Cavity content in BCII	Ligands in BCII	Corresponding content in *B. fragilis*
1	Wat2	Ser41 OG, Ser57 O, Glu30 OD1	Wat2
2	Wat4	Wat5, Pro208 O, Asn42 O, Asp56 OD2, Arg91 NH2	Phe side chain
	Wat5	Wat4, Val207 O, Gly167 N	
3	Wat6	Asn180 O, Asp183 N	Wat6
4	Wat7	Thr85 OG1, Cys168 N, Wat8, His86 ND1	Asn81OD1
	Wat8	Wat7, Gly166 O, Ile154 O	Wat8
5	Wat9	Thr111 OG1, Ile84 O, Thr108 OG1, Thr108 N	Wat9
6	Wat10	Leu178 O, Asp180 O, His149 ND1	Wat10

3.4. *The apoprotein*

The apoprotein has the same overall structure as the zinc-containing holoenzyme enzyme. Differences are observed in the flexible loop connecting β_1 with β_2, which is not well defined in the 1.85 Å model, and in residues close to the active site. The largest differences in the Cα positions are observed near the active site which is more open in the apoenzyme. If those regions are excluded the r.m.s. deviation from the Zn^{II} structure is smaller than 0.3 Å.

Fig. 7 shows views of the active sites of the apo and zinc enzymes in the same orientation. The metal ligands His86, His88 and Asp90, the 174–185 loop and Arg91 are the most affected residues. Owing to the absence of the metal ion the 174–185 loop (containing Asn180 and Asp183) and the N-terminus of the helix α_1 (residues 87–93) have moved away and some of their Cα positions deviate by more than 1 Å (Fig. 8). In the holo enzyme the 174–185 loop is held by the interaction between Asp183 OD2 and the side chain of the metal ligand His86 (see above). The absence of the active-site metal ion results in a rotation of the side chain of His86

which can no longer provide the hydrogen bond necessary for the correct orientation of the loop. As a result of this movement the active site is more open in the apoenzyme. Asp90 OD2, which was interacting with Arg91 NH2 and Zn2, has moved and turned around its χ_1 in the apo enzyme and Arg91 has also significantly changed its position and it is now far from Asp90 (Asp90 OD2···Arg91 NH2 = 3.97 Å) but makes a stronger interaction with Gly209 O. Moreover, both Arg91 and Asp56 now interact with Ser41 OG which has turned around its χ_1. Thus, it can be stated that the metal ion in the *B. cereus* metallo-β-lactamase has not

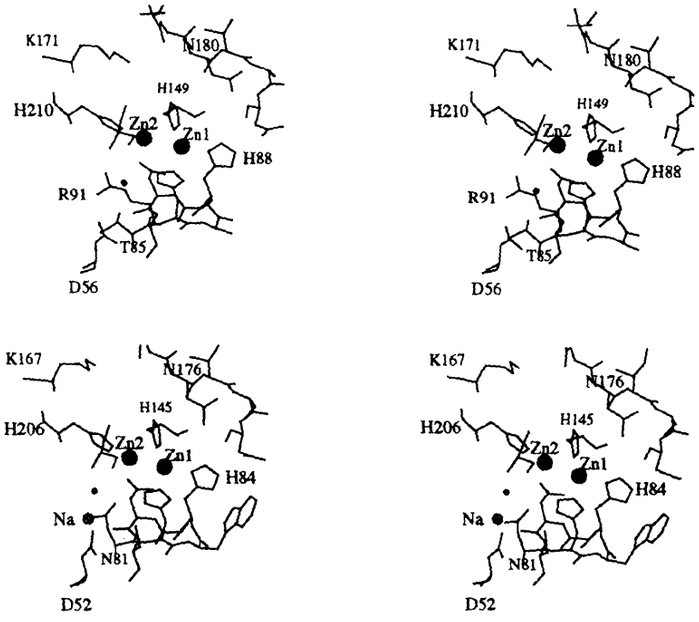

Fig. 6. Ball-and-stick representation of the active-site environment of BCII and *B. fragilis* zinc β-lactamases. The same orientation was used for the two views.

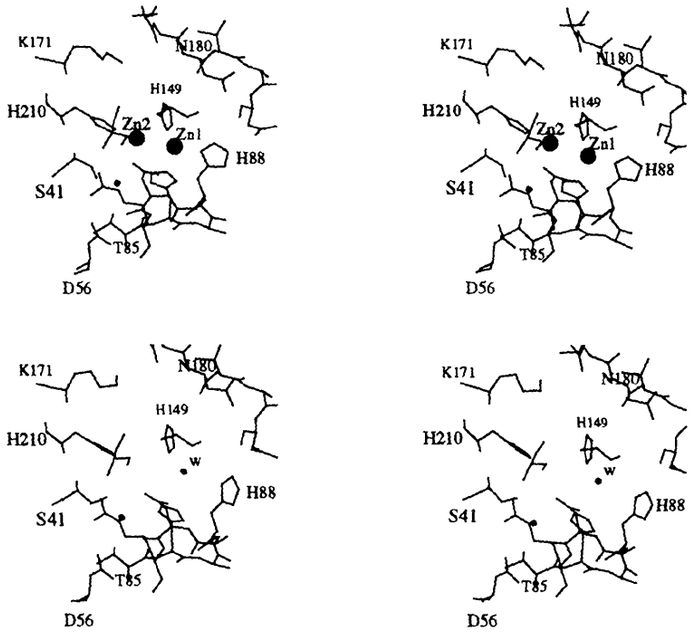

Fig. 7. Ball-and-stick representation of the active-site environment of holo and apo BCII. The same orientation was used for the two views.

only a catalytic but also a structural role. The solvation structure of the apo protein is less well defined than in the 100 K model. This results from the lower resolution of the data and the higher temperature at which data were collected. However, the majority of the described buried water molecules are conserved in the apoprotein, even if they are sometimes in slightly different positions. Wat10 is absent in the apostructure, likely as a consequence of the movement of the 174–185 loop. Furthermore a water molecule is observed in the metal-ion binding site. At the end of the refinement two strong peaks (4σ) were observed in the ($|F_o| - |F_c|, \alpha_c$) electron-density map, close to Cys168 Sγ. These peaks can be interpreted as the result of the oxidation of the cysteine residue (*i.e.* $R{-}S^- \rightarrow R{-}SO_2^-$) during the preparation of the apo crystals.

3.5. *Crystal packing*

Only one molecule (*A*) is present in the crystal asymmetric unit, which corresponds to a solvent content of 38%(*v*/*v*). Each molecule (*e.g. A*) in the crystal makes interactions with five symmetry-related molecules: three of them (*B*, *C* and *D*) are related to *A* by crystallographic twofold rotations. Thus, each specific interaction of molecule *A* with molecules *B*, *C* and *D* is present twice (Fig. 9). The fourth and fifth molecules (*E* and *F*) are related to *A* by *C* centering. Molecule *F* (not shown in Fig. 9) can be obtained by translation (**−a**, **−b**) of molecule *E*. The interactions between *A* and *E* are the same as between *F* and *A*.

It should be noted that few hydrogen bonds are made directly between protein atoms in the protein–protein contact regions. However, many water molecules are sometimes buried at these interfaces and stabilize the interaction between symmetry-related molecules through a network of hydrogen bonds with protein atoms. The interactions between molecules *A* and *B* are made mainly by residues in α_3 with those in the 174–185 loop (between β_{11} and α_4): Glu113 OE1···Glu188 OE2, Ala109 O···Asn187 ND2 and Lys117 NZ···Ala184 O. Two other hydrogen bonds are made by the carboxylate O atoms of Glu151, with Tyr185 OH and Lys147 NZ, respectively. The majority of the protein–protein interactions are found at this interface. *A* and *C* interact by their C-terminal helices (α_5) which are stacked against each other. Many water molecules buried at this interface and two salt bridges formed between His220 ND1 and Asp224 OD2, contribute to this interaction. Finally the *A*–*D* and *A*–*E* contact surfaces are large and mainly hydrophobic. The only direct protein–protein hydrogen bonds are Gln76 ND2···Lys99 O, Arg78 NE···Arg101 O, Val79 O···Arg78 NH1···Glu72 OE2 between *A* and *D* and Asn202 ND2···Tyr119 O,

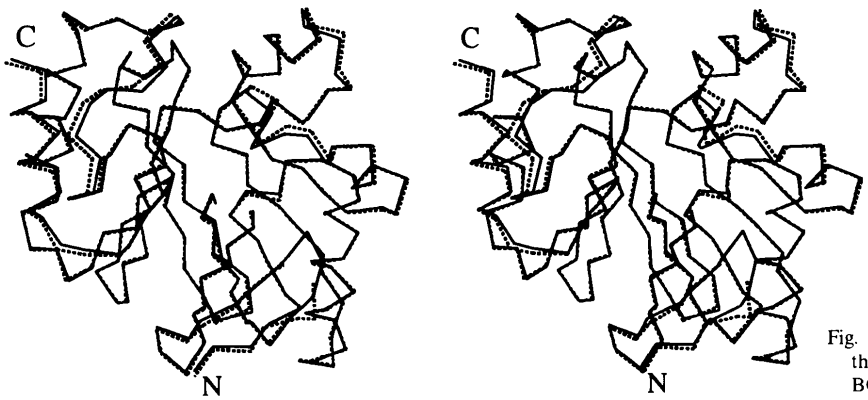

Fig. 8. Stereoview of the Cα superposition of the apo (dotted lines) and holo (solid line) BCII.

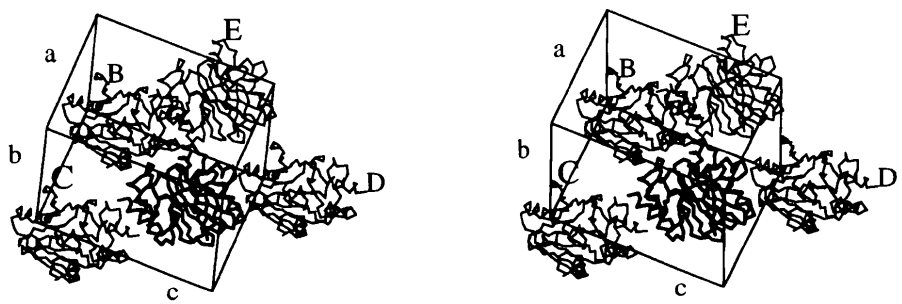

Fig. 9. Packing of the BCII molecules in the crystals. Molecule *A* is in bold, molecules *B*, *C*, *D* and *E* are labeled (see text). Lower case letters label the unit-cell edges.

Gln160 O···Lys96 NZ between *A* and *E*. The packing is quite dense and even if the active site is accessible there are no large channels in the crystal. However, it is worth noting that the first four N-terminal β-strands are not stabilized by interactions with symmetrically related molecules, which agrees with the higher observed *B* factors and disorder for that region of the structure. The compact packing and the low solvent content of the crystals may explain the difficulties encountered in the preparation of isomorphous heavy-atom derivatives and the little phase improvement obtained by the *DM* solvent-flattening procedure. Indeed, the absence of a large channel in the crystal makes this crystal form unsuitable for substrate and inhibitor diffusion experiments.

3.6. *Chain mobility*

In our map no interpretable electron density was present for residues 32–39. This loop is likely to play an important role in the catalytic mechanism. We have modelled the possible movements of the loop and shown that it could cover the active-site groove and the bound substrate. Since this region borders the active site, binding of a substrate or an inhibitor could very well force these residues to adopt a more specific conformation, rendering them visible in an electron-density map. This flexible loop could actually help positioning the substrate and acting as a lid could strongly change the electrostatic environment of the active site. In both *B. fragilis* structures (Concha *et al.*, 1996; Carfi *et al.*, 1998) this loop was stabilized in an 'open' conformation by packing interactions.

4. Conclusions

The low-temperature crystal structure of the *B. cereus* metallo-β-lactamase has revealed the presence of a partially occupied second metal site. Crystallographic and solution studies at pH 7.5 (Wouters & Paul-Soto, personal communication), have shown that the affinity for this second metal ion strongly increases at higher pH values (K_d in the micromolar range). The pH-dependent ionizations of Cys168 and His210 are probably responsible for modulating the affinity of the metal for this site.

The function of the second metal is not fully understood in class B β-lactamases. The BCII activity mostly correlates with the metal binding at the high-affinity site (Davies & Abraham, 1974). Curiously the zinc β-lactamase of *B. fragilis* tightly binds two metal ions but the enzyme of *A. hydrophila* is inhibited by the second metal ion. This is not the only case of enzymes of the same family exhibiting different metal requirements [*e.g.* PPase requires between three and five metal ions for maximal activity depending on pH and enzyme source; (Heikinheimo *et al.*, 1996)]. Cryo-kinetic experiments on the cobalt-substituted BCII, in conditions where the second site is at least partially occupied and with benzylpenicillin as substrate, have shown a stabilization of the second site upon substrate binding which could indicate an interaction of the substrate with this metal. This observation is in agreement with our proposed mechanism (Carfi *et al.*, 1998).

It has been pointed out earlier (see above) that the structure of the Zn1 site is characteristic of a catalytically active zinc. Moreover, the coordination of the second zinc ion is uncommon: it is the first example of a Cys ligand in a protein bimetal centre. In the binuclear metal enzymes of known structure the metal ions are in close proximity (3.3–3.9 Å) and are bridged by a protein residue (mono or bidentately) and in most cases by a water molecule (most likely, a hydroxide ion). The shared hydroxide or a water molecule coordinated to one of the metals is supposed to act as nucleophile. However, in contrast to the mononuclear metal enzymes, structural and mechanistic information about binuclear metal enzymes is more limited and further studies are necessary to better define their catalytic mechanism.

This is publication No. 446 of the Institut de Biologie Structurale Jean-Pierre Ebel (CEA-CNRS). This work was supported by an ECC grant Human Capital and Mobility No. ERBCHRXCT930268, a French IMABIO program and the Belgian Government as part of a Pôle d'Attraction Inter-universitaire (PAI No. 19).†

† The atomic coordinates and structure factors have been deposited with the Protein Data Bank, Brookhaven National Laboratory (Reference: 1BME, R1BMESF). Free copies may be obtained through The Managing Editor, International Union of Crystallography, 5 Abbey Square, Chester CH1 2HU, England (Reference: GR0751).

References

Ambler, R. P. (1980). *Philos. Trans. R. Soc. London Ser. B*, **289**, 321–331.

Ambler, R. P., Daniel, M., Fleming, J., Hermoso, J. M., Pang, C. & Waley, S. G. (1985). *FEBS Lett.* **189**, 207–211.

Baldwin, G. S., Galdes, A., Hill, H. A. O., Smith, B. E., Waley, S. G. & Abraham, E. P. (1978). *Biochem. J.* **175**, 441–447.

Brünger, A. T. (1992*a*). *X-PLOR Version 3.1: A system for X-ray crystallography and NMR*, Yale University Press, New Haven, Connecticut, USA.

Brünger, A. T. (1992*b*). *Nature (London)*, **355**, 472–475.

Carfi, A., Duée, E., Paul-Soto, R., Galleni, M., Frère, J.-M. & Dideberg, O. (1998). *Acta Cryst.* D**54**, 47–57.

Carfi, A., Pares, S., Duée, E., Galleni, M., Duez, C., Frère, J.-M. & Dideberg, O. (1995). *EMBO J.* **14**, 4914–4921.

Collaborative Computational Project, Number 4 (1994). *Acta Cryst.* D**50**, 760–763.

Concha, N. O., Rasmussen, B. A., Bush, K. & Herzberg, O. (1996). *Structure*, **4**, 823–836.

Davies, R. B. & Abraham, E. P. (1974). *Biochem. J.* **143**, 129–135.

Fonzé, E., Charlier, P., To'Th, Y., Vermeire, M., Raquet, X., Dubus, A. & Frère, J.-M. (1995). *Acta Cryst.* D**51**, 682–694.

Heikinheimo, P., Lehtonen, J., Baykov, A., Lahti, R., Cooperman, B. S. & Goldman, A. (1996). *Structure*, **4**, 1491–1508.

Herzberg, O. (1991). *J. Mol. Biol.* **217**, 701–719.

Hussain, M., Carlino, A., Madonna, M. J. & Lampen, J. O. (1985). *J. Bacteriol.* **164**, 223–229.

Hutchinson, E. G. & Thornton, J. M. (1990). *Proteins*, **8**, 203–212.

Jelsch, C., Mourey, L., Masson, J.-M. & Samama, J.-P. (1993). *Proteins*, **16**, 364–383.

Jones, T. A., Zou, J.-Y., Cowan, S. W. & Kjeldgaard, M. (1991). *Acta Cryst.* A**47**, 110–119.

Kabsch, W. (1988). *J. Appl. Cryst.* **21**, 916–924.

Kato, C., Kudo, T., Watanabe, K. & Horikoshi, K. (1985). *J. Gen. Microbiol.* **131**, 3317–3324.

Kelly, J. A., Didcberg, O., Charlier, P., Wery, J.-P., Libert, M., Moews, P. C., Knox, J. R., Duez, C., Fraipont, C., Joris, B., Dusart, J., Frère, J.-M. & Ghuysen, J.-M. (1986). *Science*, **231**, 1429–1431.

Knox, J. R. (1995). *Antimicrob. Agents Chemother.* **39**, 2593–2601.

Knox, J. R. & Moews, P. C. (1991). *J. Mol. Biol.* **220**, 435–455.

Kraulis, P. J. (1991). *J. Appl. Cryst.* **24**, 946–950.

Lamzin, V. S. & Wilson, K. S. (1993). *Acta Cryst.* D**49**, 129–147.

Laskowski, R. A., MacArthur, M. W., Moss, D. S. & Thornton, J. M. (1993). *J. Appl. Cryst.* **26**, 283–291.

Lobkovsky, E., Moews, P. C., Liu, H., Zhao, H., Frère, J.-M. & Knox, J. R. (1993). *Proc. Natl Acad. Sci. USA*, **90**, 11257–11261.

Massida, O., Rossolini, G. M. & Satta, G. (1991). *J. Bacteriol.* **173**, 4611–4617.

Neu, H. C. (1992). *Science*, **257**, 1064–1073.

Oefner, C., D'Arcy, A., Daly, J. J., Gubernator, K., Charnas, R. L., Heinze, I., Hubschwerlen, C. & Winkler, F. K. (1990). *Nature (London)*, **343**, 284–288.

Osano, E., Arakawa, Y., Wacharotayankun, R., Ohta, M., Horii, T., Ito, H., Yoshimura, F. & Kato, N. (1994). *Antimicrob. Agents Chemother.* **38**, 71–78.

Ramachandran, G. N., Ramakrishnan, C. & Sasisekharan, V. (1963). *J. Mol. Biol.* **7**, 95–99.

Rasmussen, B. A., Gluzman, Y. & Tally, F. P. (1990). *Antimicrob. Agents Chemother.* **34**, 1590–1592.

Rodgers, D. W. (1994). *Structure*, **2**, 1135–1140.

Samraoui, B., Sutton, B. J., Toddy, R. J., Artymiuk, P. J., Waley, S. G. & Phillips, D. C. (1986). *Nature (London)*, **320**, 378–380.

Spratt, B.G. (1975). *Proc. Natl Acad. Sci. USA* **72**, 2999–3003.

Strynadka, N. C. J., Adachi, H., Jensen, S. E., Johns, K., Sielecki, A., Betzel, C., Sutoh, K. & James, M. N. G. (1992). *Nature (London)*, **359**, 700–705.

Thompson, J. S. & Malamy, M. H. (1990). *J. Bacteriol.* **172**, 2584–2593.

Vallee, B. L. & Auld, D. S. (1993). *Proc. Natl Acad. Sci. USA*, **90**, 2715–2718.

Walsh, T. R., Hall, L., Assinder, S. J., Nichols, W. W., Cartwright, S. J., MacGowan, A. P. & Bennett, P. M. (1994). *Biochim. Biophys. Acta*, **1218**, 199–201.